UNIVERSIDADE ESTADUAL DE CAMPINAS
SISTEMA DE BIBLIOTECAS DA UNICAMP
REPOSITÓRIO DA PRODUÇÃO CIENTIFICA E INTELECTUAL DA UNICAMP

Versão do arquivo anexado / Version of attached file:

Versão do Editor / Published Version

Mais informações no site da editora / Further information on publisher's website:

https://ieeexplore.ieee.org/document/8377995

DOI: 10.1109/JPHOT.2018.2846200

Direitos autorais / Publisher's copyright statement:

Loss Compensation in Microring-Based Si Photonics Devices via Er3+ Doped Claddings

Paulo Felipe Jarschel [ID]**, Mario C. M. M. Souza, Rafael Borges Merlo, and Newton C. Frateschi**

Device Research Laboratory, Applied Physics Department, Gleb Wataghin Physics Institute, University of Campinas—UNICAMP, 13083-859 Campinas, Brazil

Abstract: We propose and demonstrate a method to compensate insertion losses in Si photonics devices based on ring resonators fabricated in SOI foundries, with no additional chip area used. It consists in the employment of $Er:Al_2O_3$ as the upper cladding layer on standard Si/SiO_2 rings, requiring only one simple post-processing step. The method is modeled in detail, and simulation results for single-ring configurations and photonic molecules are discussed, where the potential for loss reduction is predicted for different design choices based on the quality factor. We experimentally verify the viability of the method, obtaining an output power increase of 1 dB when a single-ring resonator is pumped. This value is increased when the method is applied to devices based on photonic molecules, where a value of 2.6 dB has been measured. This is equivalent to a loss reduction potential higher than 3 dB for a photonic molecule designed to achieve a quality factor of 50000.

Index Terms: Silicon nanophotonics, waveguide devices, laser amplifiers.

1. Introduction

In recent developments in the field of silicon photonics circuits, one building block of particular interest is the ring resonator, often used to filter, route, and generally control the flow of signals [1], [2]. Other demonstrated applications include, but are not limited to, optical logical circuits, modulators, buffers and high-order filters [3]–[6]. When add/drop ports are employed on these devices, to perform signal routing for example, insertion losses are always present [7]. Additionally, coupled rings (Photonic Molecules) have been extensively studied for device applications with specific spectral responses [8]–[12], where the filtering and signal processing characteristics can introduce undesirable losses as well [13], [14]. It is possible to minimize this effect by changing the coupling strength between the rings and the feeding/extracting waveguides, though this leads to a decreased quality factor (Q) and the consequent loss of filtering resolution [15]. In a complex photonic circuit, several of these components may be cascaded, and the added losses may give rise to information deterioration. Thus, one of the challenges faced by silicon photonics is maintaining the optical power level along a complex integrated circuit that has a dense sequence of devices.
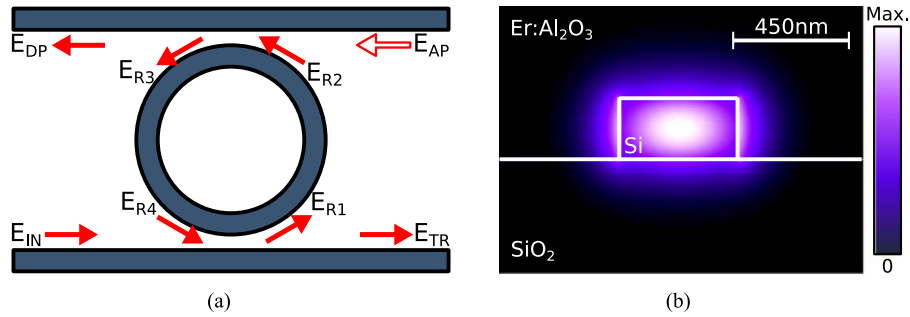
Fig. 1. (a) Schematic of a ring resonator with add/drop ports, where the electric fields amplitudes and light propagation directions are indicated at specific points. (b) FEM simulation of the quasi-TE mode of the resonator waveguide with 20 μm bending radius. The SOI waveguide is clad with Er-doped alumina film (n = 1.7).

Mimicking erbium-doped fiber amplifiers (EDFAs) functionality in the chip level is an attractive approach to help overcome this problem. To this end, erbium-doped waveguide amplifiers (EDWAs) using aluminum oxide (Al_2O_3) as the waveguide core material have been demonstrated, with net gains up to 20 dB [16], [17]. Such amplifiers benefit from high concentration of Er^{3+} ions in the Al_2O_3 matrix, up to 100 times higher than possible in SiO_2 before degrading effects occur [18]. By employing EDWAs as buffers distributed along the chip, the loss can certainly be compensated, as net gains up to 2 dB/cm have been previously reported [19], [20]. Nevertheless, these amplifiers may occupy a relatively large chip area, limiting the room for other components. Another challenge from such configurations is the process of integrating alumina waveguides to silicon photonic chips, which departs from CMOS technology and demands complex techniques to achieve reasonable coupling between the Si and Al_2O_3 waveguides [21]. A simple alternative approach consists of using a doped film as the Si waveguide top cladding. Since a considerable fraction of the propagating mode energy in single-mode silicon waveguides is outside the core, this method can allow efficient light amplification and even lasing [22]–[24]. The typical propagation loss of Si strip waveguides from SOI foundries is guaranteed to be lower than 3 dB/cm, but values as low as 1.4 dB/cm have been consistently measured [25]. This value is higher than the loss from standard Al_2O_3 EDWAs waveguides, where the refractive index contrast is smaller and thus the attenuation effect of the core walls imperfections is less pronounced. As such, the amplification potential of this approach is smaller, but still considerable, as the maximum material gain of $Er:Al_2O_3$ films has been previously reported as 2.5 dB/cm [17], [20].

In this context, we propose and demonstrate an alternative method to mitigate the insertion losses of filters and routers based on ring resonators and photonic molecules. It consists of erbium-doped alumina films as the waveguide top cladding, which can be easily employed on devices fabricated in SOI photonics foundries, with minimal post-processing.

2. Modeling

To effectively model a device with the proposed properties, we have to combine two concepts: the transfer function of ring resonators (with add/drop ports considered), and the rate equations for light amplification. Starting with the former, we can describe the fields present at each coupling area, shown in Fig. 1(a), using the transfer matrix method [26], [27], with one matrix per coupling:

$$\begin{pmatrix} E_{R1} \\ E_{TR} \end{pmatrix} = \begin{pmatrix} \tau & i\kappa \\ i\kappa & \tau \end{pmatrix} \begin{pmatrix} E_{R4} \\ E_{IN} \end{pmatrix} \tag{1}$$

$$\begin{pmatrix} E_{DP} \\ E_{R3} \end{pmatrix} = \begin{pmatrix} \tau & i\kappa \\ i\kappa & \tau \end{pmatrix} \begin{pmatrix} E_{AP} \\ E_{R2} \end{pmatrix} \tag{2}$$

$$E_{R2} = ae^{j\phi}E_{R1} \tag{3}$$

$$E_{R4} = ae^{j\phi}E_{R3} \tag{4}$$

In these equations, E represents the electric field at the points of interest indicated by the subscripts, κ and τ are respectively the field coupling and transmittance coefficients (which depend on the materials, separation gap and ring radius, obtained by the approximation from [28]), a is the ratio of change in amplitude, and ϕ the absolute phase accumulation during propagation. The optical input field (E_{IN}) is proportional to the square root of the input power, and the field at the add port (E_{AP}) is considered null. Solving Eqs. (1) through (4), the output field at the drop port is obtained as:

$$E_{DP} = E_{IN}\frac{\kappa^2 ae^{j\phi}}{(1 - \kappa^2)\, a^2 e^{2j\phi} - 1} \tag{5}$$

The amplitude variation a can be written as:

$$a = e^{-\alpha l} = e^{-\alpha\pi r} \tag{6}$$

where l is the distance traveled, corresponding to half the perimeter (distance between the two coupling regions), and α is the attenuation constant of the waveguide. In these calculations, curvature losses are not explicitly considered, but can be inserted within α. If we now consider the possibility of gain, this attenuation constant must be replaced by a value that contains the optical losses from the waveguide and the variation in optical power due to the Er ions presence in the cladding. To estimate this value, we first solve the rate equations for a typical two-level waveguide amplifier [29]:

$$\frac{dN_2}{dt} = \frac{\Gamma_p \sigma_a(\lambda_p) P_p}{hf_p A}N_1 - \frac{\Gamma_s \sigma_e(\lambda_s) P_s}{hf_s A}\left(N_2 - \frac{\sigma_a(\lambda_s)}{\sigma_e(\lambda_s)}N_1\right) - \frac{N_2}{\tau} \tag{7}$$

$$\frac{dP_s(\lambda_s)}{dz} = [g(z, \lambda_s) - \alpha]\, P_s(z) \tag{8}$$

$$\frac{dP_p(\lambda_p)}{dz} = [\eta(z, \lambda_p) - \alpha]\, P_p(z) \tag{9}$$

Here, the subscripts p, s, a and e refer to pump, signal, absorption and emission, respectively. The variables N_1 and N_2 are the fundamental and excited level population densities, so $N_1 + N_2 = N_T$. The constant Γ is the mode confinement factor, σ the erbium absorption or emission cross section, λ the photon wavelength, f the photon frequency, P the optical power, h is Planck's constant, A the waveguide transversal area, and τ is the excited state lifetime. The functions $g(z, \lambda_s)$ and $\eta(z, \lambda_p)$ are respectively the signal and pump rate of change, written as a function of both length and wavelength:

$$g(z, \lambda) = \Gamma_s[\sigma_e(\lambda) N_2(z) - \sigma_a(\lambda) N_1(z)] \tag{10}$$

$$\eta(z, \lambda) = \Gamma_p[\sigma_e(\lambda) N_2(z) - \sigma_a(\lambda) N_1(z)] \tag{11}$$

In our case, instead of using a confinement factor, we must use the overlap factor between the mode energy distribution and the Er-doped cladding. To do this, we consider a 450 nm $\times$ 220 nm single mode strip waveguide, that is, its cross-section is a rectangle surrounded by the cladding, as illustrated in Fig. 1(b). From FEM simulations performed on Comsol Multiphysics, with a 10 nm mesh, this factor was found to be 0.33 for the signal wavelength (1550 nm) and 0.3 for the pump wavelength (1480 nm), considering the quasi-TE mode. It is possible to use this same concept for rib or multi-mode waveguides, but the fraction of light that interacts with erbium ions in the cladding would be greatly reduced, impairing the loss-reduction characteristics. A slot waveguide, on the other hand, would be optimal for this application, due to the fact that the majority of the energy is guided between the Si pillars, maximizing the interaction with the doped cladding.

The signal and pump wavelengths mentioned above correspond to the $^4I_{15/2} \rightarrow {}^4I_{13/2}$ transition, with a lifetime of $\sim$8 ms. If the steady state ($dN_2/dt = 0$) is reached, numerically solving Eqs. (7)
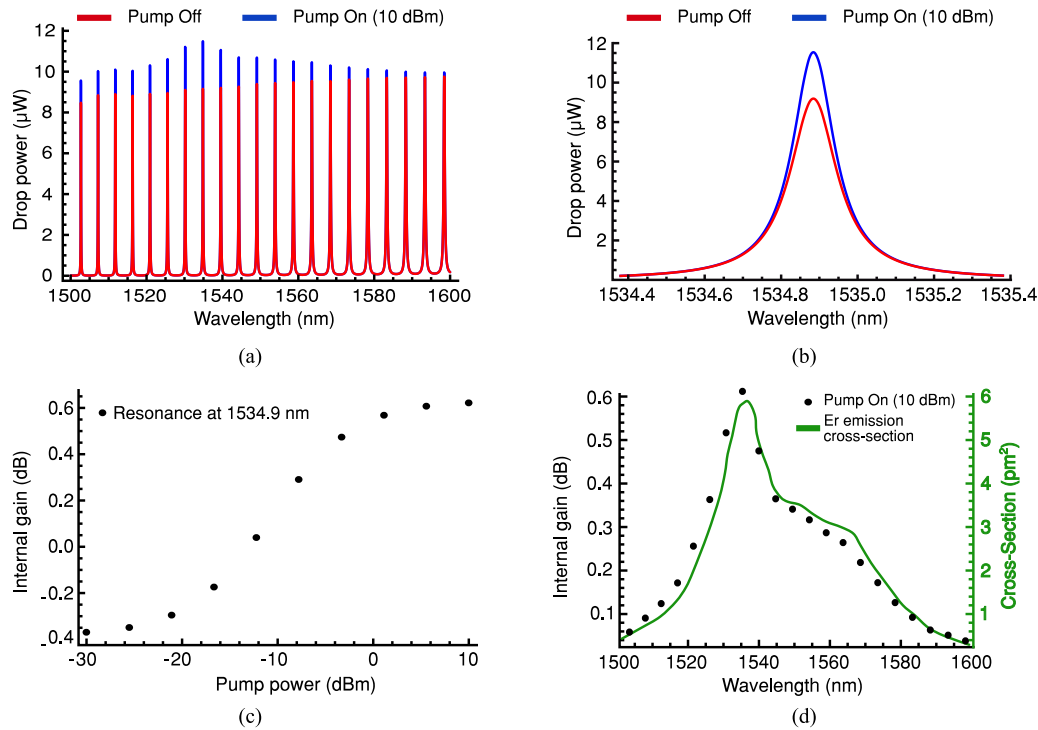
Fig. 2. Simulated device performance. (a) Drop-port spectra for On (10 mW, blue) and Off (red) pump conditions. (b) Detail of one resonance. (c) Total internal gain for the 1534.9 nm resonance as a function of pump power. (d) Spectral internal gain, compared with the Er emission cross-section used as the model input.

through (11) with $P(0) = P_0$ yields the signal power in function of the length z, in the form:

$$P(z) = P_0 e^{2\xi z} \tag{12}$$

where ξ is defined as a gain or attenuation constant. The ratio between the output and input power, equal to the ratio between the modulus squared of the output and input fields, is:

$$\frac{P(z)}{P_0} = \frac{|E(z)|^2}{|E_0|^2} = e^{2\xi z} \Rightarrow |E(z)| = |E_0|\, e^{\xi z} \tag{13}$$

By rearranging the terms, we can define the gain/attenuation constant as:

$$\xi = \frac{1}{2z} \ln\left(\frac{P(z)}{P_0}\right) \tag{14}$$

By comparing Eqs. (6) and (13), we can replace $-\alpha$ by ξ from Eq. (14) to couple both models. This gives us the complete description of the device output at the drop port, with the changes due to the Er-doped layer properly considered. One important detail to mention is that this coupling assumes that the pump laser is always present within the ring, and does not decay significantly after each roundtrip. To overcome this limitation, it is possible to calculate the finesse (F) factor of the cavity, which is related to the average number of roundtrips a photon completes before exiting the ring. It is defined by the free spectral range (distance between the resonances) divided by the resonance bandwidth. We can then estimate the pump attenuation from the rate equations considering this effective length, and the model will still be valid if the pump power is then increased by this value. For the results shown below, however, this was not necessary, as the pump attenuation was found to be less than 1 dB.

From this model, the output spectra at the drop port (E_{DP}) shown in Fig. 2(a) and Fig. 2(b) were analytically obtained using typical values for the Er concentration (5×10^{20} cm^{-3}) and

absorption/emission cross-sections (0.6 pm^2, varies with wavelength) [30]. The dimensions and materials considered are the same as the devices we fabricated: 20 μm of ring radius, 450 nm $\times$ 220 nm waveguide, and 200 nm of gap between the ring and bus waveguides, with a propagation loss of 1.5 dB/cm. Finally, an input signal of 10 μW and pump powers up to 10 mW were chosen for these results. We can observe the influence of the doped material in the output spectra, and the signal enhancement, defined as $10 log \left(P_{PumpOn} / P_{PumpOff} \right)$, is as high as 0.98 dB at the 1534.9 nm resonance when the pump is turned on (Fig. 2(b)). The quality factor is defined as the ratio between the stored energy and average loss per roundtrip, and can be obtained by the ratio between the central wavelength and the width of the respective resonance. For the resonances shown, $Q \approx 10^4$, showing an increase of 12% when the ring is pumped (10000 to 11200 for the 1534.9 nm resonance), due to loss reduction.

By varying the pump power and comparing the output from this resonance with the input, we observe optical gain from -10 dBm upwards, saturating at 0.61 dB of total internal gain (Fig. 2(c)). This shows that in theory our modeled device can not only completely compensate the insertion loss for this design, but also provide a small gain under these conditions. The lowest internal gain value (-0.37 dB, when the pump is completely off) represents the insertion loss of the device, composed of the propagation losses, absorption by the ground state Er^{3+} ions, and residual power coupling back to the input bus waveguide. When considering an undoped Al$_2$O$_3$ cladding (Er concentration $= 0$), we obtain 0.20 dB of loss, from which we can confirm that the presence of Er^{3+} ions can introduce additional loss when not pumped.

If we now take the saturated gain for each resonance, we see that it varies with the wavelength (as does the Er emission cross-section, which is an input of the model), and the peak performance is at the 1535 nm region (Fig. 2(d)). This shows that both concepts were successfully coupled on the developing of this model.

Considering a photonic molecule as the one illustrated in Fig. 3(a), where internally coupled auxiliary rings are present, additional resonances corresponding to the internal rings are created in the spectrum. These present a higher Q factor arising from the coupled system response, where more energy from the outer ring is coupled to the inner rings, instead of being extracted by the bus waveguide, effectively reducing loss. The eventual splitting of common resonances between the rings (analogous to the splitting in atomic coupling levels) can present an even higher Q ($\sim 2 \times 10^5$), as the energy accumulation effect is even stronger [11]. Such high Q factors on a small footprint (20 μm $\times$ 20 μm) make this type of device attractive for signal processing [13], [14], and consequentially a method to reduce the insertion loss is desirable. In the context of the model presented above, the addition of internally coupled rings can be represented simply by inserting extra matrices for each of the coupling areas, where the external ring acts as the bus waveguide for the internal rings. Due to the extensive length, these equations will be omitted from this text.

Considering the previous parameters, and internal rings with approximately 5 μm of radius separated from the external rings by 200 nm, the spectra for the resonances between 1553 nm and 1560 nm are shown in Fig. 3(b). The inset shows the doublet from the internal rings in detail. A small difference in the ring radius simulates fabrication imprecisions that lead to a Vernier effect, and for this case, although very small, curvature losses have been considered (0.005 dB/turn, or 0.003 dB/rad) [31]. It is important to remember that the model assumes a constant pump power along the entire device, thus all rings are considered to be pumped (1480 nm), and we can observe the signal enhancement for all the resonances. For the leftmost doublet peak, the output power increases 3.61 dB, more than the outer ring counterpart. This value, however, remains lower than the input power (5 μW, versus 10 μW). This is explained by the same reason responsible for higher quality factors, that is, a lower coupling between the light trapped in the inner rings and the bus waveguides, so less energy is extracted via the drop port. The average Q factor for the doublet resonances shown is in the order of 10^5, which results in an enhanced loss reduction potential in comparison with a single ring, due to the longer time that a photon remains trapped in the rings, analogous to a longer amplifier.
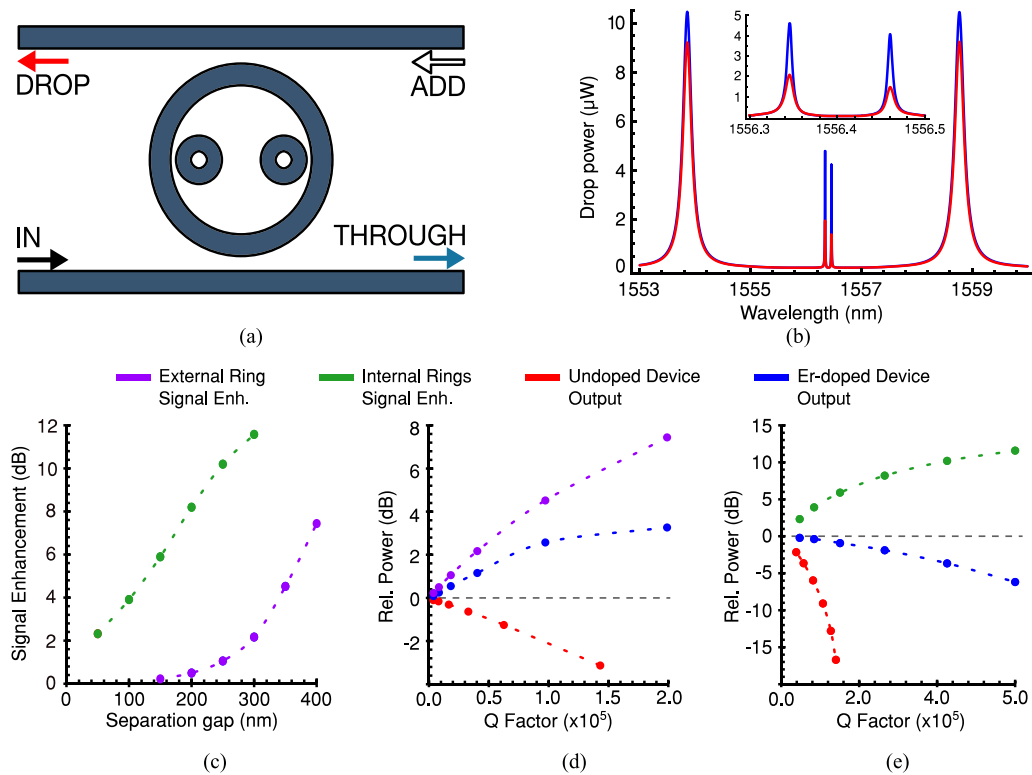
Fig. 3. (a) Schematic of a ring resonator with add/drop ports and two additional internal rings (5.1 μm radius) separated from the external by a gap of 200 nm. (b) Drop-port spectra for On (10 mW, blue) and Off (red) pump conditions. (c) Signal enhancement versus separation gap for different rings resonances. (d) Signal enhancement and output powers for the external ring resonance, as a function of the Q factor, for an Er-doped and an undoped device. (e) Signal enhancement and output powers for an internal ring resonance, as a function of the Q factor, for an Er-doped and an undoped device.

We can compare the signal enhancement values for resonances from the different rings (1554 nm for the external ring, 1556 nm for the internal rings), in function of the separation gap. Confirming the previous result, it is shown in Fig. 3(c) that the resonance from an internal ring tend to present a higher signal enhancement due to the higher Q. The effective reduction in the dissipated energy inside the rings leads to an additional increase in the quality factor, compared to a standard (undoped) device. In Figs. 3(d) and 3(e), the signal enhancement is plotted for different Q factors resulted from the different gap distances in Fig. 3(c). The difference between the output and input powers, in dB, can also be obtained in function of the quality factor, and the results for both resonances are also shown in Figs. 3(d) and 3(e). These results consider saturated Er-doped devices (1 W of pump power), in addition to the undoped devices. For the single ring resonance, the difference in output power between the Er-doped and undoped cases is higher than 5 dB for a Q factor of 1.5×10^5, corresponding to gap distances of 350 nm and 400 nm, respectively (very close to the critical coupling condition). Although the obtained gain is small, the effective loss reduction for a device presenting this Q factor is much higher. This means that from a device design point of view, it is possible to obtain a ring resonator with high Q, insertion loss (at the drop-port) reduced by 5 db, and possibly a small gain. When the resonance from an internal ring is considered, this effect is more pronounced, and although we still have losses, these are considerably lower when an Er-doped cladding is used. For the same Q factor (1.5×10^5), the insertion loss is higher than 15 dB, and decreases to less than 1 dB for an Er-doped device, resulting in a loss reduction of ~15 dB. The insertion losses increase rapidly as the Q factor increases, as seen in the red curve from Fig. 3(e). For a value of 5×10^5, the total attenuation is reduced to only 5 dB, from an extrapolated

initial value of more than 30 dB. These quality factors are equivalent to bandwidths of 1.25 GHz (1.5×10^5) and 0.37 GHz (5×10^5).

In short, these results show that the proposed method potentially enables applications of compact high-Q devices based on photonic molecules, such as routers or narrow bandpass filters where low insertion losses and reduced chip area usage are important considerations. For this particular design, Q factors in the order of 10^5 are achievable in devices occupying an area of 1257 μm^2 and with mode volumes of 18.7 μm^3.

3. Experimental Results and Discussion

To experimentally demonstrate the proposed method, we start with unclad chips containing samples of Si ring resonators manufactured by a SOI photonics foundry (IMEC), via standard CMOS-compatible processes. The devices consisted of an external ring (20 μm radius), with two smaller rings (5 μm of designed radius) internally coupled, as seen in Fig. 4(a) and Fig. 4(b). The only post-processing steps required are the deposition of the Er-doped Al$_2$O$_3$ film on top of the whole chip via co-sputtering, and a thermal annealing at 800 °C for 30 min [32]. To serve as a control sample, we deposited an undoped Al$_2$O$_3$ film on top of one of the chips. It is worth noticing that on photonic circuits, cladding changes can lead to additional losses at interfaces, and thus the fabrication process must ensure a high-quality film to minimize the attenuation, which can be caused by reflections due to gaps in the film, for example. Since our film covers the entire chip, this is not an issue for this work.

The setup shown in Fig. 4(c) was used to measure the output spectra. Two counter-propagating tunable lasers are employed: one for the signal, which is coupled to the device via a micro-lensed fiber after passing through a circulator (28 dB of isolation, 1.5 dB of insertion loss), and another for the pump, which also passes through a circulator with the same characteristics before being coupled to the ring from the drop port. The coupling loss depends on a polishing procedure performed on both sides of the chip, and for the presented results is estimated to be between 5 dB and 8 dB. The polarization must be carefully adjusted for proper coupling with the waveguide, as an inverted taper optimized for the TE mode is present at the edge; this is done with standard fiber polarization controllers. On one side of the chip, the signal exits the device via the drop port, is coupled to the lensed fiber (the same as the pump input), circulates to an optical filter that reduces by 30 dB the level of any trace pump leaked from the circulator, and is finally measured in a photodetector. On the other side, the remaining pump exits through the signal input, and is monitored with another photodetector after passing through the circulator. The lasers and photodetectors are computer controlled.

The first measurement performed was the verification of signal enhancement. The signal laser is pulsed (duration of 150 μs, repeated at 4 KHz), and tuned to a resonance at 1548.5 nm, with a peak power of 100 μW (30 μW estimated at the ring input). The pump laser was tuned to the 1476.2 nm resonance (external ring), with 10 mW of CW power. By observing the drop port output signal with an oscilloscope, we were able to measure an increase of 0.4 dB within the pulse when the pump was turned on (Fig. 4(d)). The absence of any observable increase on the noise floor indicates that the signal enhancement is not residual light from amplified spontaneous emission (ASE). The fact that the ASE is so low can be explained by the filtering characteristics of the component, since most of the spontaneous emission will occur inside the ring.

The second experiment involves sweeping the signal wavelength and measuring the output power at the drop port, maintaining the pump wavelength at the external ring resonance (1476.2 nm). The input power was set to 30 μW, and estimated to be 10 μW at the ring input. This resulted in the spectra shown in Fig. 5(a), where the response at the pump wavelength region is also displayed for reference. The first point to observe is that the resonances from the internal rings have a much lower output power, as in the simulated case. The second point, is that for the external ring resonance near 1535 nm, there is a clear difference in behavior between the doped and control (undoped) samples (Fig. 5(b)). When the doped sample is pumped (10 dBm at the chip input, estimated 5 dBm at the ring input), there is an increase in output power of 1 dB, while in the undoped sample no
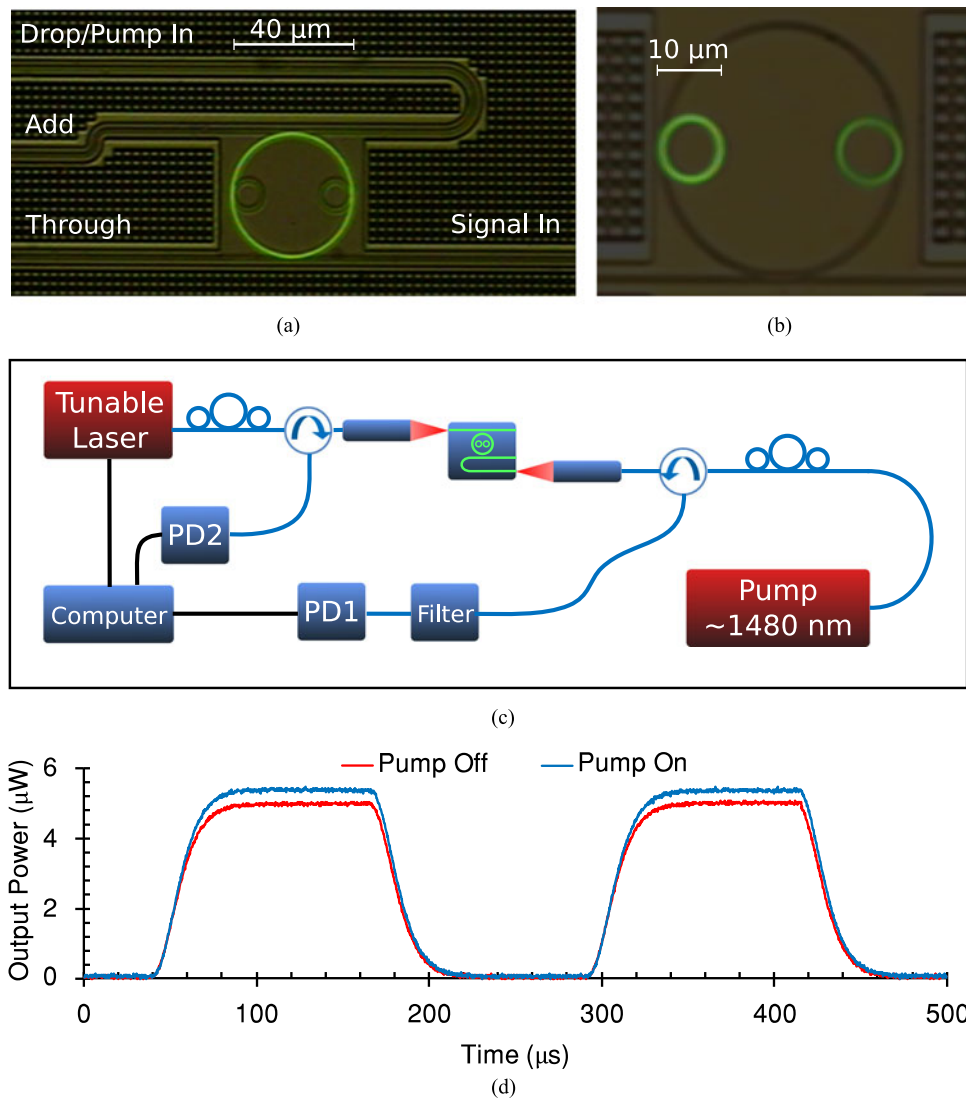
Fig. 4. Fabricated device and indicated ports when the outer ring is pumped (a), and when the inner rings are pumped (b). (c) Schematic of the measurement setup. PD: photodetector; Filter: band-pass optical filter; P.C.: polarization controller; Circ.: circulator. (d) Verification of signal enhancement by pulsing the signal laser.

increase is observed. This shows that the increase in output power is due to the erbium emission, and is not reminiscent light from the pump. In both cases, there is a red-shift in the resonance, mainly caused by thermal effects [33]. Since the inner rings are not pumped if the pump wavelength is set to an external ring resonance, the increase in output power in Fig. 5(a) for the indicated inner ring resonances is very small. However, by tuning the pump wavelength to 1479.6 nm, the inner ring resonance corresponding to the picture in Fig. 4(b), we can observe an increase of 2.6 dB for the 1556.5 nm resonance, as shown in the right portion of Fig. 5(b).

If we now vary the pump power, the successive increase in output can be measured for different resonances, as shown in Fig. 5(c). Since it is not trivial to know the exact propagation and coupling losses for the device, we cannot present the results as total gain or loss. Instead, we plot the result as the signal enhancement, defined by the ratio between the pumped and un-pumped output powers, in dB. This can also be interpreted as a loss reduction, and increases with the pump power.
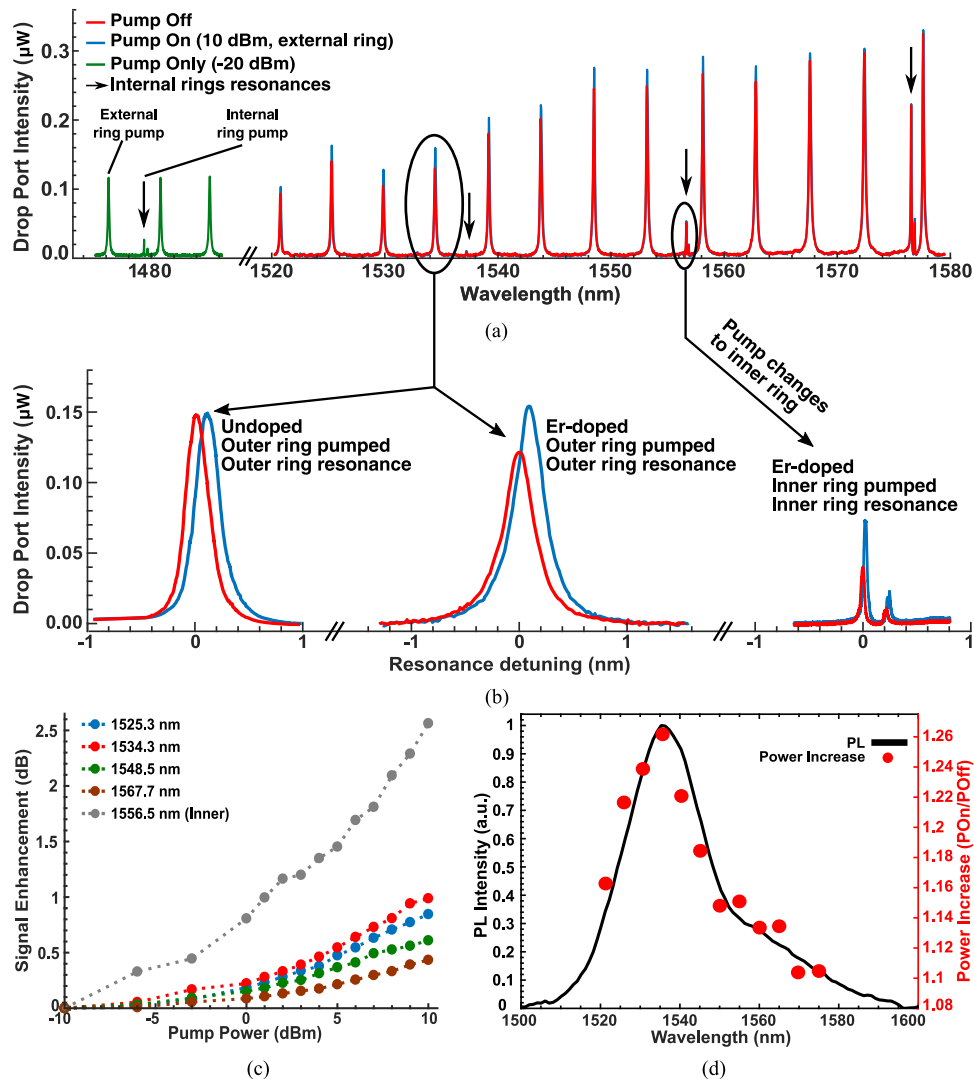
Fig. 5. Experimental results. (a) Broadband drop-port spectra for a doped device, including the system response for the pump wavelength region. (b) Comparison between undoped and doped samples, and the resonance at 1556.5 nm in detail. (c) Signal enhancement vs. Pump Power for various resonances. (d) Photoluminescence measurement (solid black line) and output power increase for all resonances within the 1520–1580 nm range (red dots).

No saturation can be observed, possibly due to the coupling losses reducing the effective pump and signal powers inside the ring, compared to the simulations. The signal enhancement can be significantly higher for the internal ring resonances (gray curve in Fig. 5(c)), reaching 2.6 dB, as opposed to 1 dB for the external ring. If the output power of the inner rings resonances near 1578 nm is measured, it is clear that it is higher than the value from the 1556.5 nm resonance, that presents the highest signal enhancement. This happens due to small differences between designed and fabricated dimensions (<100 nm in 31 μm of perimeter), leading to a Vernier effect that results in the higher proximity between the inner and outer rings resonances at higher wavelengths. As the proximity increases, light trapped in the inner ring tend to have a higher chance of coupling to the external ring, and consequently exiting via the drop port. By careful design and fabrication, or active control [34], it is possible to increase the output power of an inner ring resonance within the loss-reducing bandwidth by bringing it closer to an outer ring resonance. However, the Q factor of such resonance will at the same time decrease (from 4×10^4 to 2×10^4 for the measured
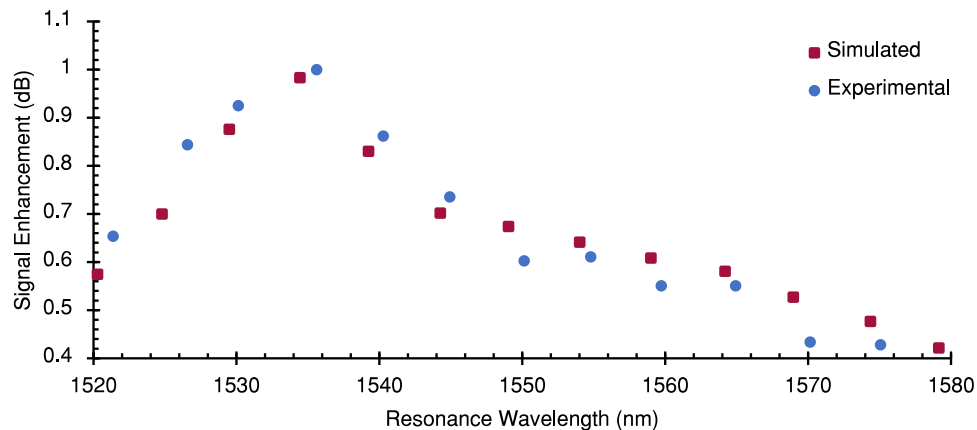
Fig. 6. Comparison between the maximum signal enhancements obtained experimentally and from simulations, in function of the resonance wavelength.

resonances in question), so a trade-off exists, and an optimal design can be obtained for the intended application.

As a final observation from the experiment, the signal enhancement is spectrally inhomogeneous and reproduces the emission spectrum of the Er-doped cladding (Fig. 5(d)). In this figure, the red dots are the enhancement at maximum pump power while the solid line shows the measured photoluminescence spectrum of the cladding film. Comparing the results from Fig. 5(d) with those in Fig. 2(d), we observe that the predictions from our model are consistent with the experimental data, as Fig. 6 shows. The measured signal enhancement deviates only 2% from the calculated value at the highest point (1535 nm region), and the behavior when varying the resonance wavelength is equivalent for both the modeled and measured results. For the inner ring resonance, the difference in the signal enhancement is higher (3.6 dB vs. 2.6 dB, not shown in the graph), which can be explained by additional losses in the rings coupling regions, also responsible for a lower Q factor for the fabricated dimensions. The measured Q factor for this resonance was 5×10^4 (4×10^4 when unpumped), which would be equivalent of a loss reduction from 3.65 dB to 0.3 dB, according to the results in Fig. 3(e). Although this net loss is clearly not reached experimentally, the measured signal enhancement is consistent with the value from the same figure (2.5 dB).

This gives us more confidence in the model developed, although the cause for additional losses in the coupling regions (with increased effect for higher Q factors, due to the additional roundtrips) need to be investigated. One possibility is the non-conformal film that results from the co-sputtering deposition method.

Additional differences between the calculated and experimental results can be mainly attributed to distinct input powers considered, a possible variation of erbium concentration and Al_2O_3 film refractive index along the sample, and the eventual small fabrication variations that may lead to different coupling strengths and considerable resonant wavelength shifts. To illustrate the latter effect, a 1% difference in the ring radius can lead to a deviation greater than 100 pm.

All the presented results consider a very high Er concentration ($5 \times 10^{20} cm^{-3}$), which degrades the stimulated emission potential [35], as can be seen by the strong green luminescence from pumped rings (also visible to the naked eye). To counteract this effect, the film can be co-doped with Ytterbium, enabling higher effective ion concentrations and thus higher gain potential. With a high-Q cavity, this can lead to the design and fabrication of amplifiers and lasers based on Er/Yt-doped materials [36]. Additionally, the employment of slot waveguides on photonic molecules, which greatly enhances the overlap between the mode energy and Er-doped cladding [24], can create the possibility of even more compact lasers on silicon with CMOS compatible technologies.

4. Conclusion

We proposed and demonstrated a method to assist in overcoming insertion losses of silicon photonics devices, such as filters and routers, based on ring resonators. It is especially useful in complex routing circuits, where many rings are concatenated. Whereas regular amplifying methods employ EDWAs that can occupy precious chip real-estate, our proposal is an effective approach to loss reduction without the need for any additional area sacrifice. As a final remark, this method of resonant amplification enables the design and fabrication of compact high-Q devices that occupy a reduced chip area and present acceptable insertion losses, as opposed to high-Q rings with larger radius, or standard photonic molecules with lower output power on high-Q resonances.

Acknowledgment

References

[1] W. Bogaerts *et al.*, "Silicon microring resonators," *Laser Photon. Rev.*, vol. 6, no. 1, pp. 47–73, 2012.

[2] S. Feng, T. Lei, H. Chen, H. Cai, X. Luo, and A. Poon, "Silicon photonics: From a microresonator perspective," *Laser Photon. Rev.*, vol. 6, no. 2, pp. 145–177, 2012.

[3] Y. Tian *et al.*, "Proof of concept of directed OR/NOR and AND/NAND logic circuit consisting of two parallel microring resonators," *Opt. Lett.*, vol. 36, no. 9, pp. 1650–2, May 2011.

[4] G. T. Reed, G. Mashanovich, F. Y. Gardes, and D. J. Thomson, "Silicon optical modulators," *Nature Photon.*, vol. 4, p. 660, Sep. 2010.

[5] F. Xia, L. Sekaric, and Y. Vlasov, "Ultracompact optical buffers on a silicon chip," *Nature Photon.*, vol. 1, p. 65, Dec. 2006.

[6] B. E. Little *et al.*, "Very high-order microring resonator filters for WDM applications," *IEEE Photon. Technol. Lett.*, vol. 16, no. 10, pp. 2263–2265, Oct. 2004.

[7] M. Dasic and M. A. Popovic, "Minimum drop-loss design of microphotonic microring-resonator channel add-drop filters," in *Proc. 20th Telecommun. Forum*, Nov. 2012, pp. 927–930.

[8] L. Zhang, M. Song, T. Wu, L. Zou, R. G. Beausoleil, and A. E. Willner, "Embedded ring resonators for microphotonic applications," *Opt. Lett.*, vol. 33, no. 17, pp. 1978–1980, Sep. 2008.

[9] X. Zhou, L. Zhang, A. M. Armani, R. G. Beausoleil, A. E. Willner, and W. Pang, "Power enhancement and phase regimes in embedded microring resonators in analogy with electromagnetically induced transparency," *Opt. Exp.*, vol. 21, no. 17, pp. 20 179–20 186, Aug. 2013.

[10] Y. Hu *et al.*, "High-speed silicon modulator based on cascaded microring resonators," *Opt. Exp.*, vol. 20, no. 14, pp. 15 079–15 085, Jul. 2012.

[11] L. A. M. Barea, F. Vallini, G. F. M. de Rezende, and N. C. Frateschi, "Spectral engineering with CMOS compatible SOI photonic molecules," *IEEE Photon. J.*, vol. 5, no. 6, pp. 2 202 717–2 202 717, Dec. 2013.

[12] S. V. Boriskina, I. Chremmos, O. Schwelb, and N. Uzunoglu, *Photonic Molecules and Spectral Engineering*. Boston, MA, USA: Springer, 2010.

[13] M. C. M. M. Souza, L. A. M. Barea, F. Vallini, G. F. M. Rezende, G. S. Wiederhecker, and N. C. Frateschi, "Embedded coupled microrings with high-finesse and close-spaced resonances for optical signal processing," *Opt. Exp.*, vol. 22, no. 9, pp. 10 430–10 438, May 2014.

[14] L. A. M. Barea, F. Vallini, P. F. Jarschel, and N. C. Frateschi, "Silicon technology compatible photonic molecules for compact optical signal processing," *Appl. Phys. Lett.*, vol. 103, no. 20, 2013, Art. no. 201102.

[15] A. Vorckel, M. Monster, W. Henschel, P. H. Bolivar, and H. Kurz, "Asymmetrically coupled silicon-on-insulator microring resonators for compact add-drop multiplexers," *IEEE Photon. Technol. Lett.*, vol. 15, no. 7, pp. 921–923, Jul. 2003.

[16] A. Polman, "Exciting erbium-doped planar optical amplifier materials," in *Proc. SPIE*, vol. 3942, 2000, pp. 3942-1–3942-12, 2000.

[17] S. A. Vázquez-Córdova *et al.*, "Erbium-doped spiral amplifiers with 20 db of net gain on silicon," *Opt. Exp.*, vol. 22, no. 21, pp. 25 993–26 004, Oct. 2014.

[18] G. N. van den Hoven, E. Snoeks, A. Polman, C. van Dam, J. W. M. van Uffelen, and M. K. Smit, "Upconversion in erimplanted Al2O3 waveguides," *J. Appl. Phys.*, vol. 79, no. 3, pp. 1258–1266, 1996.

[19] G. N. van den Hoven, R. J. I. M. Koper, A. Polman, C. van Dam, J. W. M. van Uffelen, and M. K. Smit, "Net optical gain at 1.53 μm in erdoped Al$_2$O$_3$ waveguides on silicon," *Appl. Phys. Lett.*, vol. 68, no. 14, pp. 1886–1888, 1996.

[20] J. D. B. Bradley, L. Agazzi, D. Geskus, F. Ay, K. Wörhoff, and M. Pollnau, "Gain bandwidth of 80 nm and 2 dB/cm peak gain in Al2O3:Er3+ optical amplifiers on silicon," *J. Opt. Soc. Amer. B*, vol. 27, no. 2, pp. 187–196, Feb. 2010.

[21] L. Agazzi *et al.*, "Monolithic integration of erbium-doped amplifiers with silicon-on-insulator waveguides," *Opt. Exp.*, vol. 18, no. 26, pp. 27 703–27 711, Dec. 2010.

[22] A. Tengattini *et al.*, "Toward a 1.54 μm electrically driven erbium-doped silicon slot waveguide and optical amplifier," *J. Lightw. Technol.*, vol. 31, no. 3, pp. 391–397, Feb. 2013.

[23] C. A. Barrios and M. Lipson, "Electrically driven silicon resonant light emitting device based on slot-waveguide," *Opt. Exp.*, vol. 13, no. 25, pp. 10 092–10 101, Dec. 2005.

[24] D. Korn *et al.*, "Lasing in silicon-organic hybrid waveguides," *Nature Commun.*, vol. 7, p. 10864, Mar. 2016.

[25] I. Aldaya, A. Gil-Molina, J. L. Pita, L. H. Gabrielli, H. L. Fragnito, and P. Dainese, "Nonlinear carrier dynamics in silicon nano-waveguides," *Optica*, vol. 4, no. 10, pp. 1219–1227, Oct. 2017.

[26] A. Yariv, "Universal relations for coupling of optical power between microresonators and dielectric waveguides," *Electron. Lett.*, vol. 36, no. 4, pp. 321–322, Feb. 2000.

[27] J. Heebner, R. Grover, and T. Ibrahim, *Optical Microresonators: Theory, Fabrication and Applications.* New York, NY, USA: Springer, 2008.

[28] B. E. Little, S. T. Chu, H. A. Haus, J. Foresi, and J. P. Laine, "Microring resonator channel dropping filters," *J. Lightw. Technol.*, vol. 15, no. 6, pp. 998–1005, Jun. 1997.

[29] R. Hui and M. O'Sullivan, *Fiber Optic Measurement Techniques.* New York, NY, USA: Academic Press, 2009.

[30] G. N. van den Hoven, J. A. van der Elsken, A. Polman, C. van Dam, K. W. M. van Uffelen, and M. K. Smit, "Absorption and emission cross sections of Er3+ in Al2O3 waveguides," *Appl. Opt.*, vol. 36, no. 15, pp. 3338–3341, May 1997.

[31] Y. A. Vlasov and S. J. McNab, "Losses in single-mode silicon-on-insulator strip waveguides and bends," *Opt. Exp.*, vol. 12, no. 8, pp. 1622–1631, Apr. 2004.

[32] P. F. Jarschel, M. C. M. M. Souza, A. A. G. V. Zuben, A. C. Ramos, R. B. Merlo, and N. C. Frateschi, "Enabling III-V integrated photonics with Er-doped Al2O3 films," in *Proc. 2014 29th Symp. Microelectron. Technol. Dev.*, Sep. 2014, pp. 1–4.

[33] A. Arbabi and L. L. Goddard, "Dynamics of self-heating in microring resonators," *IEEE Photon. J.*, vol. 4, no. 5, pp. 1702–1711, Oct. 2012.

[34] M. C. M. M. Souza, G. F. M. Rezende, L. A. M. Barea, A. A. G. von Zuben, G. S. Wiederhecker, and N. C. Frateschi, "Spectral engineering with coupled microcavities: Active control of resonant mode-splitting," *Opt. Lett.*, vol. 40, no. 14, pp. 3332–3335, Jul. 2015.

[35] P. G. Kik and A. Polman, "Cooperative upconversion as the gain-limiting factor in Er doped miniature Al2O3 optical waveguide amplifiers," *J. Appl. Phys.*, vol. 93, no. 9, pp. 5008–5012, 2003.

[36] J. D. B. Bradley and E. S. Hosseini, "Monolithic erbium- and ytterbium-doped microring lasers on silicon chips," *Opt. Exp.*, vol. 22, no. 10, pp. 12 226–12 237, May 2014.